On-chip quasi-digital optical switch using silicon microring resonator-coupled Mach-Zehnder interferometer

Junfeng Song,[1,2,*] Xianshu Luo,[1] Xiaoguang Tu,[1] Lianxi Jia,[1] Qing Fang,[1] Tsung-Yang Liow,[1] Mingbin Yu,[1] and Guo-Qiang Lo[1]

[1]*Institute of Microelectronics, A*STAR (Agency for Science, Technology and Research), 11 Science Park Road, Science Park II, Singapore 117685, Singapore*

[2]*State Key Laboratory on Integrated opto-electronics, College of Electronic Science and Engineering, Jilin University, Changchun 130012, China*

songjf@ime.a-star.edu.sg

Abstract: In this work, we demonstrate thermo-optical quasi-digital optical switch (q-DOS) using silicon microring resonator-coupled Mach-Zehnder interferometer. The optical transmission spectra show box-like response with 1-dB and 3-dB bandwidths of ~1.3 nm and ~1.6 nm, respectively. Such broadband flat-top optical response improves the tolerance to the light source wavelength fluctuation of ± 6 Å and temperature variation of ± 6 °C. Dynamic characterizations show the device with switching power of ~37 mW, switching time of ~7 μs, and on/off ratio of > 30 dB. For performance comparison, we also demonstrate a carrier injection-based electro-optical q-DOS by integrating lateral P-i-N junction with the microring resonator, which significantly reduces power consumption to ~12 mW and switching time to ~0.7 ns only.

OCIS codes: (130.3120) Integrated optics devices; (130.4815) Optical switching devices; (130.2790) Guided waves; (220.0220) Optical design and fabrication; (220.4000) Microstructure fabrication; (230.0230) Optical devices; (230.3990) Micro-optical devices.

References and links

1. H. Zimmermann, *Integrated Silicon Optoelectronics* (Springer, 2000).
2. L. Pavesi, "Will silicon be the photonic material of the third millenium?" J. Phys. Condens. Matter **15**(26), R1169–R1196 (2003).
3. B. Jalali, S. Yegnanarayanan, T. Yoon, T. Yoshimoto, I. Rendina, and F. Coppinger, "Advances in silicon-on-insulator optoelectronics," IEEE J. Sel. Top. Quantum Electron. **4**(6), 938–947 (1998).
4. R. Soref, "The past, present, and future of Silicon photonics," IEEE J. Sel. Top. Quantum Electron. **12**(6), 1678–1687 (2006).
5. G. I. Papadimitriou, C. Papazoglou, and A. S. Pomportsis, "Optical switching: switch fabrics, techniques, and architectures," J. Lightwave Technol. **21**(2), 384–405 (2003).
6. T. S. A. El-Bawab, *Optical switching* (Springer Verlag, 2006)
7. R. J. Bates, *Optical switching and networking handbook* (McGraw-Hill, Inc., 2001).
8. Y. Silberberg, P. Perlmutter, and J. E. Baran, "Digital optical switch," Appl. Phys. Lett. **51**(16), 1230–1232 (1987).
9. Y. O. Noh, J. M. Kim, M. S. Yang, H. J. Choi, H. J. Lee, Y. H. Won, and S. G. Han, "Thermooptic 2× 2 asymmetric digital optical switches with zero-voltage operation state," IEEE Photon. Technol. Lett. **16**(2), 446–448 (2004).
10. K. Jinguji and M. Kawachi, "Synthesis of coherent two-port lattice-form optical delay-line circuit," J. Lightwave Technol. **13**(1), 73–82 (1995).
11. K. Jinguji, "Synthesis of coherent two-port optical delay-line circuit with ring waveguides," J. Lightwave Technol. **14**(8), 1882–1898 (1996).
12. A. W. Poon, X. Luo, F. Xu, and H. Chen, "Cascaded microresonator-based matrix switch for silicon on-chip optical interconnection," Proc. IEEE **97**(7), 1216–1238 (2009).
13. X. Luo, J. Song, S. Feng, A. Poon, T. Y. Liow, M. Yu, G. Q. Lo, and D. L. Kwong, "Silicon high-order coupled-microring-based electro-optical switches for on-chip optical interconnects," IEEE Photon. Technol. Lett. **24**(10), 821–823 (2012).
14. J. Song, Q. Fang, S. H. Tao, M. B. Yu, G. Q. Lo, and D. L. Kwong, "Proposed silicon wire interleaver structure," Opt. Express **16**(11), 7849–7859 (2008).

#183461 - $15.00 USD Received 14 Jan 2013; revised 4 Mar 2013; accepted 5 Mar 2013; published 16 May 2013

15. J. Song, Q. Fang, S. H. Tao, M. B. Yu, G. Q. Lo, and D. L. Kwong, "Passive ring-assisted Mach-Zehnder interleaver on silicon-on-insulator," Opt. Express **16**(12), 8359–8365 (2008).
16. J. Song, S. H. Tao, Q. Fang, T. Y. Liow, M. B. Yu, G. Q. Lo, and D. L. Kwong, "Thermo-optical enhanced silicon wire interleavers," IEEE Photon. Technol. Lett. **20**(24), 2165–2167 (2008).
17. J. Song, H. Zhao, Q. Fang, S. H. Tao, T. Y. Liow, M. B. Yu, G. Q. Lo, and D. L. Kwong, "Effective thermo-optical enhanced cross-ring resonator MZI interleavers on SOI," Opt. Express **16**(26), 21476–21482 (2008).
18. Q. Fang, J. F. Song, T. Y. Liow, H. Cai, M. B. Yu, G. Q. Lo, and D. L. Kwong, "Ultralow power silicon photonics thermo-optic switch with suspended phase arms," IEEE Photon. Technol. Lett. **23**(8), 525–527 (2011).
19. J. Song, Q. Fang, S. H. Tao, T. Y. Liow, M. B. Yu, G. Q. Lo, and D. L. Kwong, "Fast and low power Michelson interferometer thermo-optical switch on SOI," Opt. Express **16**(20), 15304–15311 (2008).

1. Introduction

Silicon-on-insulator (SOI) based photonics has huge application potential enabling the implementation of high density, multi-functional photonic integrated circuits, and also hybrid opto-electronic integrated circuits [1–4]. Optical switch is the one of the fundamental building blocks in photonic switching system [5–7], such as optical cross connect (OXC), wavelength selective switch (WSS), reconfigurable optical add-drop multiplexer (ROADM). These are widely applied in optical communications and optical interconnects.

Most of the on-chip integrated optical switches, the optical transfer response (spectra or intensity) are slowly changing with electrical signals. We name them as analog optical switch (AOS). Generally, the structures are as Mach-Zehnder interferometer (MZI) and microring. Figure 1(a) shows the working principle of such AOS. Suppose that the carrier wavelength sitting at the peak wavelength, the intensity at the carrier wavelength gradually reduces due to the voltage supplying induced peak wavelength red shift. The intensity according to the applied voltage is plotted in Fig. 1(b). In such case, the switching on/off ratio depends on the wavelength shift. The longer the wavelength shift is, the higher the on/off ratio is. However, the maximum on/off ratio equals the extinction ratio. In such AOS, the switching performances tend to be infected by the light source wavelength fluctuation, the fabrication imperfection induces wavelength shift, and the temperature variation, as the performance is sensitive to the carrier wavelength. Such problem can be overcome by adopting digital optical switch (DOS) with *step-like response* to the switching voltage [8]. General DOS structures include X-crossing [9] or Y-branches [9]. Such DOS is with the advantages of wavelength, polarization and temperature insensitive, and non-periodic, yet with high electrical power consumption and large footprint, thus being not feasible for on-chip opto-electrical integrated circuit (OEIC). In practice, a *boxlike tunable optical filter* can be used as a switch, with the performance similar to a DOS. Here we name it as quasi-digital optical switch (q-DOS). Furthermore, it is can be made with compact footprint and low power consumption. Figure 1(c) schematically illustrates the working principle of a q-DOS. The optical intensity remains the maximum until the edge of the passband reaches the carrier wavelength, and the intensity suddenly changes from the maximum to the minimum. Figure 1(d) shows the intensity change upon the applied voltage. In such case, the switch on/off ratio equals the extinction ratio. Furthermore, it is with improved tolerance to the light source wavelength fluctuation, the resonance misalignment, and the temperature change, as long as the carrier wavelength remains inside the passband, that is denoted as $\Delta\lambda$ in Fig. 1(c).

Thus, comparing to the conventional AOS, such q-DOS is with the following advantages: i) Large tolerance to the light source wavelength fluctuation, ii) Large tolerance to the temperature variation, iii) large tolerance to the fabrication imperfection induced wavelength misalignment, and iv) High immunity to the electrical signal disturbance.

#183461 - $15.00 USD Received 14 Jan 2013; revised 4 Mar 2013; accepted 5 Mar 2013; published 16 May 2013

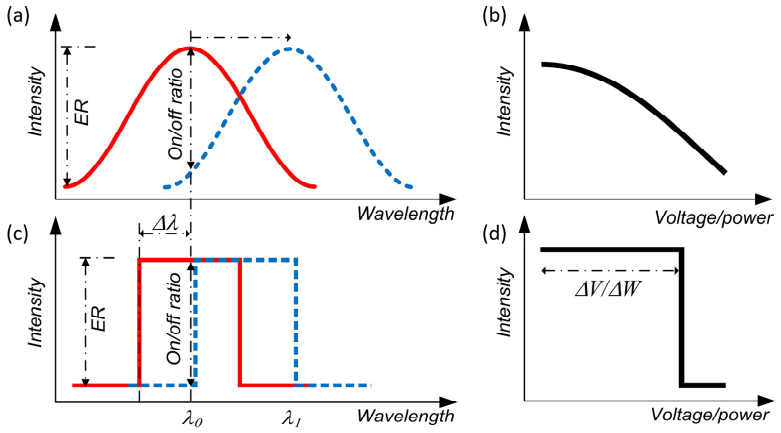

Fig. 1. The working principle comparison between an AOS and a q-DOS. (a) - (b) Optical switching of an analog switch. (c) - (d) Optical switching of a digital switch.

There are different structures for realizing such q-DOS, including multi-stage MZI structure [10], microring coupled multi-stage MZI structure [11], and coupled ring-resonator optical waveguides (CROWs) [12,13]. However, it always requires dynamic adjustment to make up the wavelength misalignment by using tunable technique considering the fabrication variation. Thus, it could be difficult to use multi-stage structure since every stage needs to be tuned simultaneously. Previously, we have demonstrated two kinds of microring coupled MZI structure-based interleavers with flat-top broadband passband [14, 15]. We also observed that the thermo-optical tuning on the 3-dB directional coupler improves the device significantly [16, 17].

In this work, by integrating the thermo-optical (TO) function to the microring resonator, we demonstrate TO q-DOS. The transmission spectra show broadband flat-top response with 1-dB and 3-dB bandwidths of ~1.3 nm and 1.6 nm, respectively. The measured switching power is ~37 mW and switching time is ~7 μs with up to 30 dB on/off ratio. Furthermore, for performance comparison, we also integrate lateral PIN diode with the microring resonator to demonstrate a carrier-injection based electro-optical (EO) q-DOS with low power consumption and fast switching speed. However, such EO q-DOS is with increased optical loss and decreased on/off ratio.

2. Device fabrication and characterization

2.1 Fabrications

In this work, we design and implement the q-DOS in silicon-on-insulator (SOI) platform by using CMOS-compatible fabrication process. The SOI wafer is with a 220 nm silicon layer on a 2 μm buried oxide (BOX) layer. The device is patterned by 248 nm DUV photolithography and a two-step silicon reactive ion etching (RIE) to form a rib waveguide for ion implantation and a channel waveguide for the nano-taper. The slab for the ion implantation is ~60 nm thick. The lateral PIN diode of the microring is formed by ion implantation in the slab layer. The implants are activated using rapid thermal anneal of 1050 °C for 5 seconds. A 1 μm-thick oxide layer is deposited, followed by the formation of TiN thermal heater. Subsequently, another 500 nm insulating oxide is deposited, and separate contact holes to the Si implantation regions and the thermal heater are opened. This is followed with Al metallization. Finally, ~100 μm Si deep trench is etched in order for the light butt-coupling between the lensed optical fiber and the inverse taper waveguide.

Figures 2(a)-2(b) show the design of waveguide structures of the TO and EO q-DOS using microring resonator-coupled MZI structure, while Figs. 2(c)-2(d) show the optical microscope images of the fabricated devices. For both TO and EO q-DOS, the two arms of the MZI are designed identically in length, suggesting a symmetric MZI. The passband tunability is

#183461 - $15.00 USD Received 14 Jan 2013; revised 4 Mar 2013; accepted 5 Mar 2013; published 16 May 2013

achieved by changing the refractive index of the microring resonator, respectively via the temperature change induced from the thermal heater and the carrier injection of the lateral P-i-N junction. We also integrate thermal heaters to both 3-dB direction couplers in the MZI in order to achieve high-performance 3-dB direction coupling. Furthermore, we adopt 500 nm waveguide for the TO switch in order for low insertion loss, while designing 400 nm waveguide for the EO switch as the EO performance directly relates to the waveguide width. The rest of the design parameters, including the coupling length, microring circumference, etc, are subsequently determined. In such microring switches, the directional coupler parameters are critical. We design all gaps of the directional couplers to be 300 nm. For the gap between the waveguide and the microring, we target the coupling coefficients of 0.414, corresponding to the coupling length of 60 μm and 12 μm, respectively for TO and EO devices. The lengths of 3-dB directional coupler are 40 μm and 7.4 μm. The bend radius in the microring resonators are designed to be 10 μm.

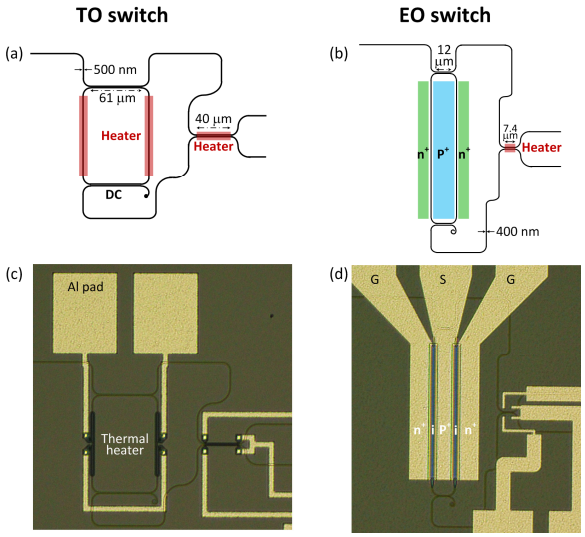

Fig. 2. (a) - (b) Design layouts of the TO-tunable and EO-tunable q-DOS using microring resonator-coupled MZI structures. (c) - (d) The optical microscope images of the fabricated devices.

2.2 Results and discussion

The device characterizations include the transmission measurements upon different DC voltage supply and the dynamic testing of the switch response. Figure 3(a) shows the setup for the transmission measurement, we adopt a wideband amplified spontaneous emission (ASE, EXFO FLS-2300B) and a laser diode as the light source, following with a polarization controller before ending firing to the silicon waveguide using polarization maintaining lensed fiber. The output intensity is collected by another single mode lensed fiber and recorded by an optical spectrum analyzer (OSA, ANDO AQ6317B). Two DC power suppliers are adopted for the voltage supplying to the microring and the directional coupler.

#183461 - $15.00 USD Received 14 Jan 2013; revised 4 Mar 2013; accepted 5 Mar 2013; published 16 May 2013

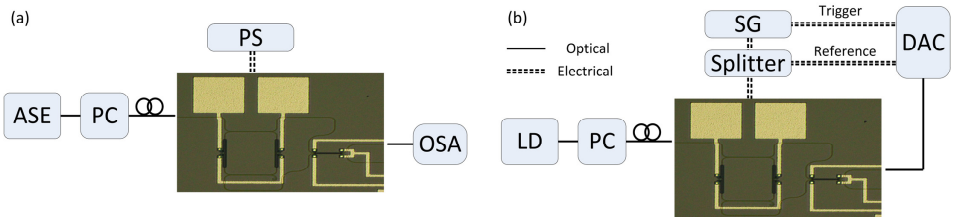

Fig. 3. Characterization setups for (a) optical transmission measurement, and (b) switching dynamic response measurement. LD: laser diode. PC: polarization controller. PS: power supply. SG: signal generator. DCA: digital communications analyzer.

Figure 3(b) shows the switch dynamic response measurement setup. A continue laser sitting at the probe wavelength is used as the light source. The optical switches are driven using a radio frequency (RF) signal. The output signal is displayed by using a digital communication analyzer (DCA, Agilent 86100C). In order for comparison, we also use an electrical splitter to split the electrical driving and display the electrical signal in the DCA. As EO and TO switches are with significantly different time responses, we adopt two different RF signal generators.

2.2.1 TO-tunable q-DOS

We first characterize the TO q-DOS. Figure 4(a) shows the measured transmission spectra upon 0 and 37 mW DC power supply. The spectra are normalized to a reference waveguide which is with ~6 dB insertion loss. The transmission loss of waveguide is only ~0.4 dB, other loss is from lensed fiber with nano taper waveguide. The extinction ratio is ~30 dB, and the on/off ratio is also ~30 dB. The high extinction ratio from the transmission spectra suggests the MZI 3-dB directional coupler to be with relatively high performance. Thus, we disable the thermal tunability of the MZI 3-dB directional coupler in our measurements. All the electrical signals mentioned hereafter are supplied to the microring resonators. Figure 4(b) shows the zoom-in view of the spectrum, illustrating the 1-dB and 3-dB bandwidth of ~1.3 nm (160 GHz) and 1.6 nm (200 GHz), respectively. This suggests that, laser wavelength tolerance is +/– 80 GHz within 1 dB range. The theoretical analysis shows the bandwidth of 1-dB and 3-dB are 0.4 FSR and 0.5 FSR, respectively [14]. As analyzed in [14], the bandwidth of the passband is determined by the microring circumference. The smaller the circumference is, the wider the FSR becomes, and thus the wider the bandwidth is. The 1-dB bandwidth can be extended to 8 nm as shown in [14] with the FSR is increased to 20 nm.

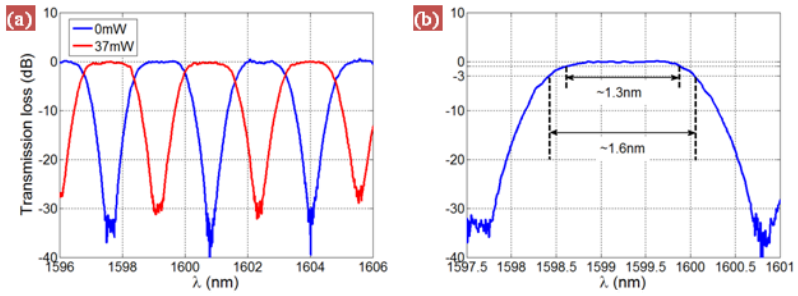

Fig. 4. (a) The measured transmission spectra for on- and off- states. The electrical powers are 0 and 37 mW, respectively. (b) Zoom-in view of a single passband illustrating 1-dB and 3-dB bandwidth of ~1.3 nm and ~1.6 nm, respectively.

For an TO device, the index of the microring increases as the temperature increases, which results in the redshift of the resonant wavelength. The blue dots in Fig. 5 show the change of the passband center wavelength as function of the applied electrical power, which exhibits a linear relationship. The red line shows the linear fitting to the experimental data, TO

#183461 - $15.00 USD Received 14 Jan 2013; revised 4 Mar 2013; accepted 5 Mar 2013; published 16 May 2013

efficiency of ~0.4 Å/mW is extracted. By using isolation trench, the TO efficiency shall be increased [18,19].

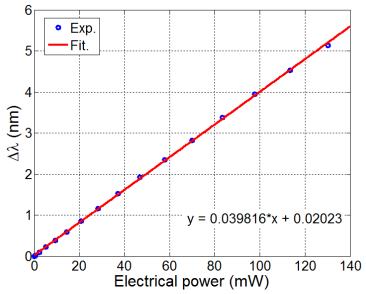

Fig. 5. Wavelength shift as the function of the electrical power. Blue circles denote experimental results. Red line is the linear fiting result.

By fixing the carrier wavelength, we can measure the optical intensity response to the applied electrical power via scanning the voltage supplied to the microring resonator. The dotted lines in Figs. 6(a) and 6(b) show the measured optical intensity response as function of applied electrical power at wavelengths of 1599.2 nm (passband center) and 1600.8 nm (stopband center). In both passbands and stopbands, the optical states is stable with electrical power change in ± 10 mW range. This suggests that, the optical response is with as large as 20 mW tolerance to the electrical disturbance. By using the theoritical analysis [14], we fit the experimental measurement, which shows good agreement.

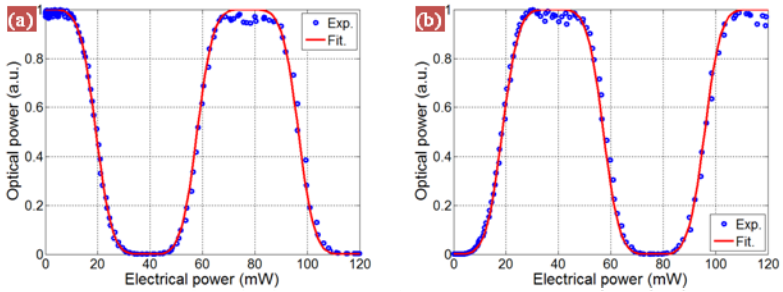

Fig. 6. Optical power change as functions of the supplied electrical power at wavelengths of (a) 1599.2 nm, and (b) 1600.8 nm.

Figures 7 (a) and 7(b) show the optical response of the TO q-DOS at the wavelength of 1599.2 nm and 1600.8 nm upon square-shaped RF signal driving to the microring resonator. The input electrical signals shown in red lines are also included as the references. In order for comparison between the electrical drive signal and the optical response, we compensate the time delay between them. The optical swicthing time (rise time + fall time) is ~7 μs. As rise/fall times of the the electrical signals are negligible, the optical switching time is limited by the heat transfer and dispation times. The switch power and switch time of TO switch are dependent on heat dissipation of device. Generally, low heat dissipation typically results in lower switching power but with longer switching time. Furthermore, we see that by selecting the probe wavelengths either at the center of the transmission band (1599.2 nm) or the center of the stop band (1600.8 nm), the rise times and the falling times are changed in the opposite way, which is due to the different optical responses to the electrical driving as shown in Fig. 1.

#183461 - $15.00 USD Received 14 Jan 2013; revised 4 Mar 2013; accepted 5 Mar 2013; published 16 May 2013

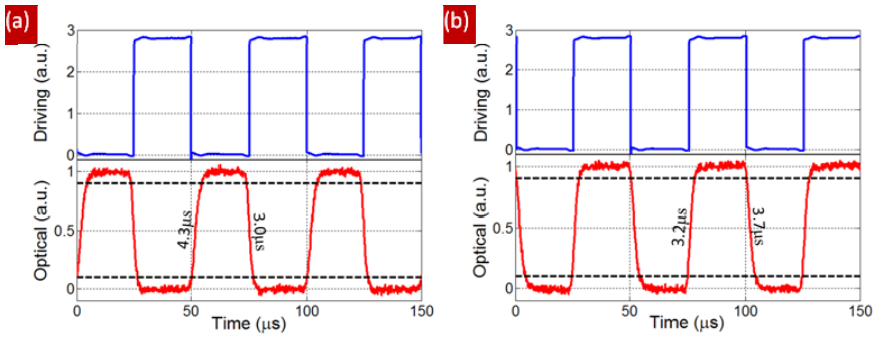

Fig. 7. The measured optical switching response upon square-shaped RF supply at wavelegths of (a) 1599.2 nm, and (b) 1600.8 nm. The dashed lines indicate the 10% and 90% intensity positions for rise/fall times measurement.

Another advantage of such q-DOS is the high tolerance to the electical power fluctuation, which would relax the demand on the quality of the input electrical signal. As an example, we show the optical response driving by a triangle-shaped electrical signal. Figure 8(a) illustrates the working principle. The green line shows the optical transmission and the red lines denote the input electrical signal. Supposing the carrier wavelength being set at the pass-band center (see Fig. 6(a)), the on-state corresponds to the low electrical input, whereas the off-state corresponds to the high electrical input. The optical output response keeps with the maximum until the band edge reaches to the carrier wavelength, then followed with minimum optical response. The sharper roll-off of the optical passband is, the faster change of the optical response becomes. Figure 8(b) shows the experimental results of such waveform transition. The input triangle-shaped signal is changed to NRZ signal with the rise time and fall time of ~6.5 μs and ~5.5 μs, respectively. We attribute such prolonged rise/fall times to the less steep change of the electrical signal.

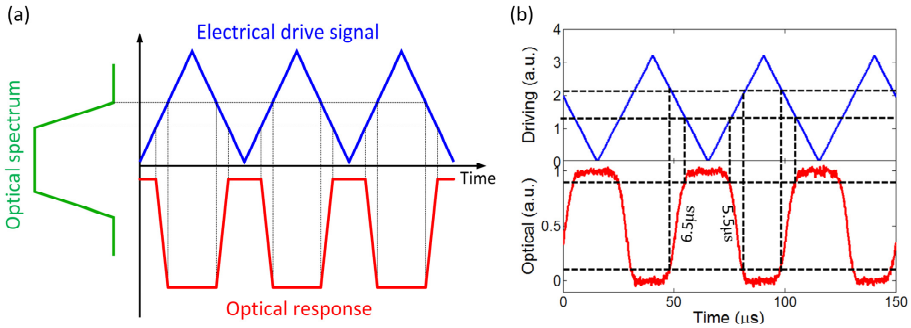

Fig. 8. (a) Schematic illustration of the working principle upon triangle-shaped RF signal input. Green line is the optical transmission. Red line is the input electrical signal. Blue line is the optical response signal. (b) Measured optical response upon the triangle-shaped RF signal driving.

Finally, we investigate the temperature dependence of such broadband digital switch using a thermo-electrical cooler (TEC). The TEC is placed under the chip in order for uniform temperature distribution. The temperature is controlled by adjusting the current. The transmission spectra upon different temperatures are recorded, as shown in Fig. 9(a). The passband shifts to longer wavelength with one period upon the temperature change of less than 20 °C. Figure 9(b) shows the resonance shift as the function of the temperature, associating with the linear fitting, which suggests ~0.11 nm wavelength red-shift per degree temperature change. We can estimate the thermo-optical coefficient of the effective refractive index change. As the microring circumference is ~385 μm and the FSR is ~3.2 nm, we obtain the group index n_g is ~4.13. The thermo-optical coefficient is 2.84×10^{-4}/°C. Considering the

#183461 - $15.00 USD Received 14 Jan 2013; revised 4 Mar 2013; accepted 5 Mar 2013; published 16 May 2013

−1 dB passband width of ~1.3 nm, the temperature tolerance of our demonstrated digital switch is ± 6 °C. Further increase the passband by reducing the microring circumference can increase the temperature tolerance.

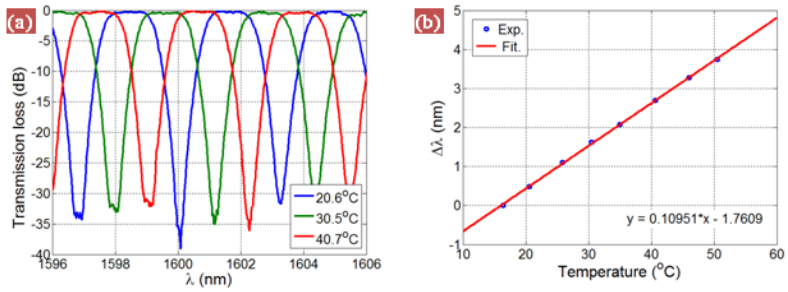

Fig. 9. (a) Optical transmission spectra with the photonic chip under different temperatures. (b) Resonance shift as the function of the temperature.

2.2.2 EO-tunable q-DOS

For performance comparison, we also report on the measurements of the EO q-DOS. Figure 10(a) shows the measured transmission spectra of the EO q-DOS from two different ports, which is normalized to the transmission of a standalone waveguide. The relative transmission loss is ~1 dB. The extinction ratio is larger than 30 dB.

The resonance blue shifts for a forward-biased P-i-N junction due to the carrier injection induced refractive index decrease. Meanwhile, due to the carrier injection, there will also be free-carrier absorption loss increasing. Figure 10(b) shows the measured transmission spectra before and after the resonance shift. The electrical power consumption for a passband shift is ~12 mW, which is three times lower than that of TO device. However, due to the free-carrier injection, the transmission loss increases to −3 dB, and the extinction ratio reduces to ~10 dB. The reduced extinction ratio is due to the unbalanced light distributions in the two MZI arms. In such case, there is a trade-off between the optical insertion loss and the switching on-off ratio. If we choose the carrier wavelength at the center of passband, the on-off ratio will be limited to ~10 dB only. On the other hand, if we choose the carrier wavelength at the center of the stop-band, there will be 2 dB additional optical transmission losses, yet with as high as ~28 dB on-off ratio.

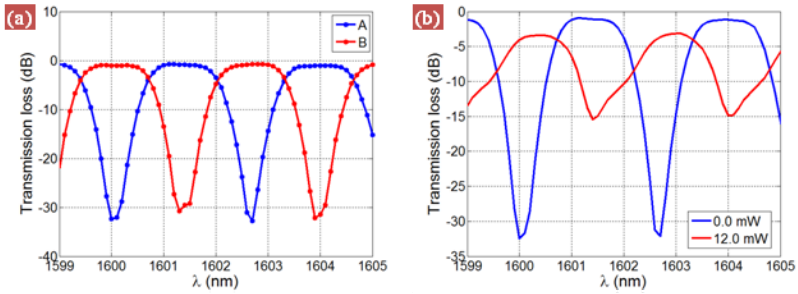

Fig. 10. (a) Measured optical transmission spectra of an EO digital switch from two output waveguides. (b) Optical transmission spectra at on and off states from output waveguide A.

Another advantage for the EO device is its fast switching speed. Figure 11 shows the optical response at wavelength of 1601.4 nm upon a square-wave drive voltage. The rise time and fall time are 350 ps and 348 ps, respectivily. As expected, this suggests orders of magnitude faster swithing speed than that in TO device.

#183461 - $15.00 USD Received 14 Jan 2013; revised 4 Mar 2013; accepted 5 Mar 2013; published 16 May 2013

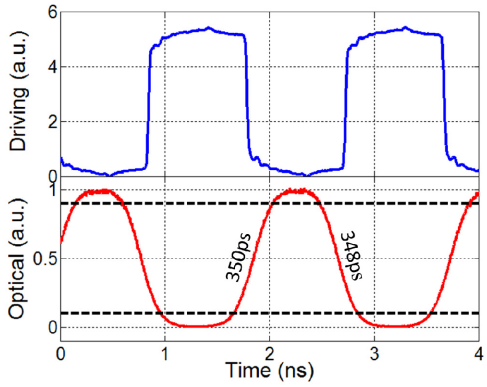

Fig. 11. Optical response of an EO digital switch upon a square-shaped RF singal driving. Both rise time and fall time are ~350 ps. The dashed lines indicate the 10% and 90% intensity positions for rise/fall times measurement.

3. Conclusion

We demonstrated thermo-optical quasi-digital optcial switch by using silicon microring resonator-coupled MZI structure. The tranmission spectra showed box-like optical reponse with 1-dB ad 3-dB bandwidths of 1.3 nm and 1.6 nm, respectively. Such broadband flat-top optical response enhanced the tolerance to the light source wavelength fluctruation to ± 6 Å and temperature variation of ± 6 °C. The switching power was ~37 mW and swithing time was ~7 μs with up to 30 dB on/off ratio. As comparison, we also demonstrated an electro-optical digital optical switch with similar design integrating a lateral P-i-N junction. Such EO digital optical switch was demonstrated with only 12 mW switching power and 0.7 nm switching time. Yet, due to the free-carrier induced optical absorption, additional loss was measured with reduced on/off ratio.

Acknowledgments

This work was supported by the Science and Engineering Research Council of A*STAR (Agency for Science, Technology and Research), Singapore, under SERC grant number 1122804038, and National Natural Science Foundation of China (NSFC, Grant No. 61177090).

#183461 - $15.00 USD Received 14 Jan 2013; revised 4 Mar 2013; accepted 5 Mar 2013; published 16 May 2013